remote sensing

MDPI

Article

Fusing Multiple Land Cover Products Based on Locally Estimated Map-Reference Cover Type Transition Probabilities

Wangle Zhang [1,2], Jiwen Wang [1,2], Hate Lin [1,2], Ming Cong [1], Yue Wan [3] and Jingxiong Zhang [4,*]

[1] College of Geological Engineering and Geomatics, Chang'an University, Xi'an 710054, China
[2] Big Data Center for Geosciences and Satellites (BDCGS), Chang'an University, Xi'an 710054, China
[3] College of Resource and Environment, Henan Agricultural University, Zhengzhou 450002, China
[4] School of Geodesy and Geomatics, Wuhan University, Wuhan 430079, China
[*] Correspondence: jxzhang@whu.edu.cn

Abstract: There are a variety of land cover products generated from remote-sensing images. However, misclassification errors in individual products and inconsistency among them undermine their utilities for research and other applications. While it is worth developing advanced pattern classifiers and utilizing the images of finer spatial, temporal, and/or spectral resolution for increased classification accuracy, it is also sensible to increase map classification accuracy through effective map fusion by exploiting complementarity among multi-source products over a study area. This paper presents a novel fusion method that works by weighting multiple source products based on their map-reference cover type transition probabilities, which are predicted using random forest for individual map pixels. The proposed method was tested and compared with three alternatives: consensus-based weighting, random forest, and locally modified Dempster–Shafer evidential reasoning, in a case study, over Shaanxi province, China. For this case study, three types of land cover products (GlobeLand30, FROM-GLC, and GLC_FCS30) of two nominal years (2010 and 2020) were used as the base maps for fusion. Reference sample data for model training and testing were collected following a robust stratified random sampling design that allows for augmenting reference data flexibly. Accuracy assessments show that overall accuracies (OAs) of fused land cover maps have been improved (1~9% in OAs), with the proposed method outperforming other methods by 2~8% in OAs. The proposed method does not need to have the base products' classification systems harmonized beforehand, thus being robust and highly recommendable for fusing land cover products.

Keywords: land cover; fusion; transition probability; error matrix; augmented sampling; accuracy; reference classification

check for updates

Citation: Zhang, W.; Wang, J.; Lin, H.; Cong, M.; Wan, Y.; Zhang, J. Fusing Multiple Land Cover Products Based on Locally Estimated Map-Reference Cover Type Transition Probabilities. *Remote Sens.* **2023**, *15*, 481. https://doi.org/10.3390/rs15020481

Academic Editor: Dino Ienco

Received: 7 October 2022
Revised: 10 January 2023
Accepted: 11 January 2023
Published: 13 January 2023

1. Introduction

Land cover is an important descriptor of the Earth's surface and one of the key variables for various research and applications. A variety of land cover products, such as the International Geosphere-Biosphere Program Data and Information System's land cover (IGBP DISCover) data product [1], the Global Land Cover 2000 (GLC2000) [2], and the Moderate Resolution Imaging Spectroradiometer (MODIS) Land Cover Type product MCD12Q1 [3] are generated from remote-sensing images of medium spatial resolution. In recent years, products with finer spatial resolution have also been produced based on Landsat series or Sentinel-2 images [4–6].

Although land cover products are often produced by applying advanced classifiers and following sophisticated protocols, their thematic accuracies may be inadequate for certain applications. There also exist semantic inconsistencies among multiple products. Accuracy assessment and consistency analysis have been the topics of continuing research (e.g., [7,8]).

For increasing accuracy, the fusion of multiple land cover products may be pursued. This aims for the harmonization and synthesis of multiple land cover maps to produce maps of improved accuracy and usability through the exploration of synergies between source products, which usually differ in spatial resolution, classification schemes, and accuracies among other things. We review some of the methods developed so far for fusing multiple land cover products, including direct association, more sophisticated harmonization, regression modeling, Dempster–Shafer evidence theory, and accuracy-based weighting to illuminate the motivations, novelty, and focus of this research.

A method was developed to merge existing products into a desired classification legend [9]. It follows the idea of convergence of evidence and generates a 'best-estimate' dataset using fuzzy agreement. The method was applied to develop a new joint 1-km global land cover product (SYNMAP) with improved characteristics for land cover parameterization of the carbon cycle models in a European model intercomparison initiative of three global vegetation models: BIOME-BGC, LPJ, and ORCHIDEE. A key feature of the SYNMAP legend is that all classes are properly defined in terms of plant functional type mixtures, which can be remotely sensed and include the definitions of the leaf type and longevity for each class with a tree component.

A general framework was proposed for building a hybrid land cover map using the synergistic combination of a number of land cover classifications with different legends and spatial resolutions [10]. As in previous studies [11], all the legends (CORINE, GLC2000, MODIS, and GlobCover) were compared in the context of the UN Land Cover Classification System (LCCS) instead of performing a direct association among them [12]. This allowed for a number of criteria mostly used in classification systems to be examined. The methodology includes three main phases: (1) translation of legends into LCCS and definition of a set of attributes, (2) calculation of an overlap metric, and (3) calculation of the affinity scores (between the target labels and the assessed labels for individual products in a pixel $\mathbf{x}$). The choice of the hybrid label is therefore made according to the weighted vote for each target class, with the weight being the conditional probabilities that pixel $\mathbf{x}$ belongs to target categories given the map class labels at pixel $\mathbf{x}$ by individual products.

A harmonization procedure was implemented using Latent Dirichlet Allocation (LDA) modeling [13]. The LDA model was based on the regionalized class co-occurrences from multiple maps to output harmonized class labels at individual pixels by statistically characterizing land attributes from the aforementioned class co-occurrences. Multiple harmonization approaches were evaluated [13]: LDA modeling alone and those in combination with error matrices and semantic affinity scores. The results were compared with the benchmark maps generated using simple legend crosswalks showing that using LDA outputs with error matrices performed better, with the harmonized map overall accuracy increased by 6–19% for areas of disagreement between the source maps.

A semi-automatic method was devised to generate two hybrid and static agricultural masks—one for cropland and another for grassland, at the 250 m spatial resolution for the nominal year 2016, based on multi-criteria analysis (MCA), complemented with manual fine-tuning using the best-rated datasets [14]. Following a comprehensive selection of land cover maps, each dataset was evaluated at the country level according to five criteria: timeliness, spatial resolution, comparison with FAO statistics, accuracy assessment, and expert evaluation. Through sensitivity analysis the impact of weight settings on the resulting land cover was evaluated. The proposed methodology [14] improved agricultural characterization in Africa.

The methods reviewed so far are mostly based on the quantifying votes of source map class labels on harmonized class labels by using direct association, affinity scores, error matrices, LDA, and MCA, combined with manual fine tuning. Another group of methods for fusion is regression modeling, as reviewed below.

Logistic regression has been used to integrate six existing global land cover maps [15], whereby 2100 ground truth data points were randomly selected as training data. For each training point, they calculated the frequency with which the land cover types used in the six original maps applied to each of the six target types (of ground truth data) was computed. The scores (probabilities of occurrences) of target classes for a land cover map were calculated and used as explanatory variables, with the ground truth data used as endogenous variables. It was found that the accuracy of the resultant harmonized map is 74.6%, being 3% higher than for existing maps. A 0.5-min latitude by 0.5-min longitude probability map was also created, indicating the probability of agreement between the class of the new map and the truth data. Using the map, it was found that the probabilities of cropland and grassland are relatively low compared with other land cover types because the definitions of cropland differ between maps. Thus, accuracy may be improved by including pasture and idle plot categories.

Geographically weighted regression (GWR) and crowdsourced validation data from Geo-Wiki were used to create two hybrid global land cover maps based on medium resolution land cover products [16]. Two different methods were used: (1) the GWR was used to determine the best land cover product at each location, and (2) the GWR was only used to determine the best land cover at those locations where all three land cover maps disagree, using the agreement of the land cover maps to determine land cover at the other cells. GWR estimates model parameters at each geographical location by using a kernel, with the observations weighted by distance. Logistic regression was used to calculate the probability of correspondence between the validation data and the global datasets at each pixel of a 300 m grid.

Using a reference dataset and four land cover products (Globcover-2009, Land Cover-CCI-2010, MODIS-2010, and Globeland30) for Africa, five LC map integration methods were tested and cross-validated [17]. Comparison of the spatial correspondences showed that the preferences for land cover maps varied spatially. Integration methods using both the maps and reference data at their locations resulted in a 4.5–13% higher correspondence with the reference classification than any of the input maps. An integrated land cover map and class probability maps were computed using regression kriging, which produced the highest correspondence (76%). The general trend of probabilities of cover types' presence were predicted using a multinomial logistic (MNL) regression model. These were locally adjusted by interpolating the indicator residuals using simple kriging. A regression kriging method was also used to integrate Globcover-2009, LC-CCI-2010, MODIS-2010, and Globeland30 maps and several publicly available reference datasets [18]. Overall correspondence of the integrated map with reference data was 80% based on a 10-fold cross-validation using 24,681 sample sites. This is globally 10% and regionally 6–13% higher than correspondences among the input maps.

Some of the most commonly-used methods to develop a hybrid forest cover map by combining available land cover/forest products and crowdsourced data on forest cover obtained through the Geo-Wiki project were compared empirically [19]. The methods compared include: nearest neighbor, naive Bayes, logistic regression, geographically-weighted logistic regression (GWR), and classification and regression trees (CART). The comparison experiments were carried out using two data types: the presence/absence of forest in a grid cell and the percentage of forest cover in a grid cell. In general, there was little difference between the methods. However, GWR was found to perform better than the other tested methods in areas with high disagreement between the inputs.

The Dempster–Shafer theory of evidence also provides a framework for fusing multiple land cover products. For example, to integrate five different products in China, at a 1 km resolution, evidence theory was applied [20], with the quantity of evidence computed via literature reviews and analyses of correlation between map classes from different classification systems.

As another example for evidence-based map fusion, an improved global land cover map for 2015 at a 30 m resolution was developed by fusing multiple existing land cover products [21]. Firstly, more than 160,000 global point-based samples were used to locally evaluate the reliability of the input products for each class within each $4^\circ \times 4^\circ$ geographical grid for the establishment of the basic probability assignment (BPA) function. Then, the Dempster's rule of combination was used for each 30 m pixel to derive the combined probability mass of each possible land cover class. Finally, each pixel was determined with a land cover class based on a decision rule. Results indicate that in the areas of inconsistency, accuracy gains in the range of 17.6–23.2% in areas of moderate inconsistency, and 21.0–25.2% in areas of high inconsistency.

A land cover map 2015 for China was generated from multiple source products using the theory of evidence and knowledge rule optimization [22]. The results showed the aforementioned method can reduce the disagreement between input data. The fused map attained a classification accuracy comparable to that of the China land use map (CNLULC), which was based on visual image interpretation, while having more thematic detail (i.e., more land cover classes). Compared with Geo-Wiki observations in 2015, the overall accuracy (OA) of the fused map is higher than the other two global land cover data.

The fourth kind of method for fusion is hereby called accuracy weighting. A global consensus land cover product with a 1 km resolution was generated using accuracy weighting [23]. Land cover classes of the consensus product at pixels with inconsistent map classes were selected as being those registering the maximum accuracy-weighted average of class memberships/proportions. The accuracies were estimated from the error matrices of different base products. It was confirmed that the fusion process should be selectively applied on heterogeneous pixels with users' accuracies (UAs) being used for weighting in map fusion.

Four cropland products, produced initially from multiple sensors (e.g., Landsat-8 OLI, Sentinel-2 MSI, and PROBA–V) to cover the period (2015–2017), were integrated based on their cropland mapping accuracy to build a more accurate cropland layer [24]. The four cropland layers' accuracy was assessed at agro-ecological zones units via an intensive reference dataset (17,592 samples). The most accurate cropland layer was then identified for each zone to construct the final cropland mask at a 30 m resolution for the nominal year of 2016 over Africa. As a result, the new layer was produced in higher cropland mapping accuracy (OA = 91.64% and cropland's F-score = 0.75).

This paper presents a novel method for fusing multiple source (base) land cover products into a new product based on their map-reference cover type transition probabilities. These transition probabilities are predicted locally through random forest (RF), a machine learning approach, and serve as the basis for weighting source products. The main hypotheses underlying this research are: (1) transition probabilities provide fuller information about map-reference cover type transitions, not just classification correctness as measured by UAs in method CON, and (2) with properly estimated local transition probabilities, the proposed method TP is expected to outperform alternative methods.

2. Materials and Methods

2.1. Study Area and Datasets

Shaanxi province, located in the middle-west of China (105°29′~111°15′E, 31°42′~39°35′N), is the study area of the research. The total area of Shaanxi province is approximately 205,600 km^2. The land cover products listed below (GlobeLand30, FROM-GLC, and GLC_FCS30) are the base products we applied for fusion. The major land cover classes of the study area are forest, cultivated land, and grassland, according to the base products. Figure 1a,b shows base products in study area for 2010 and 2020, respectively.

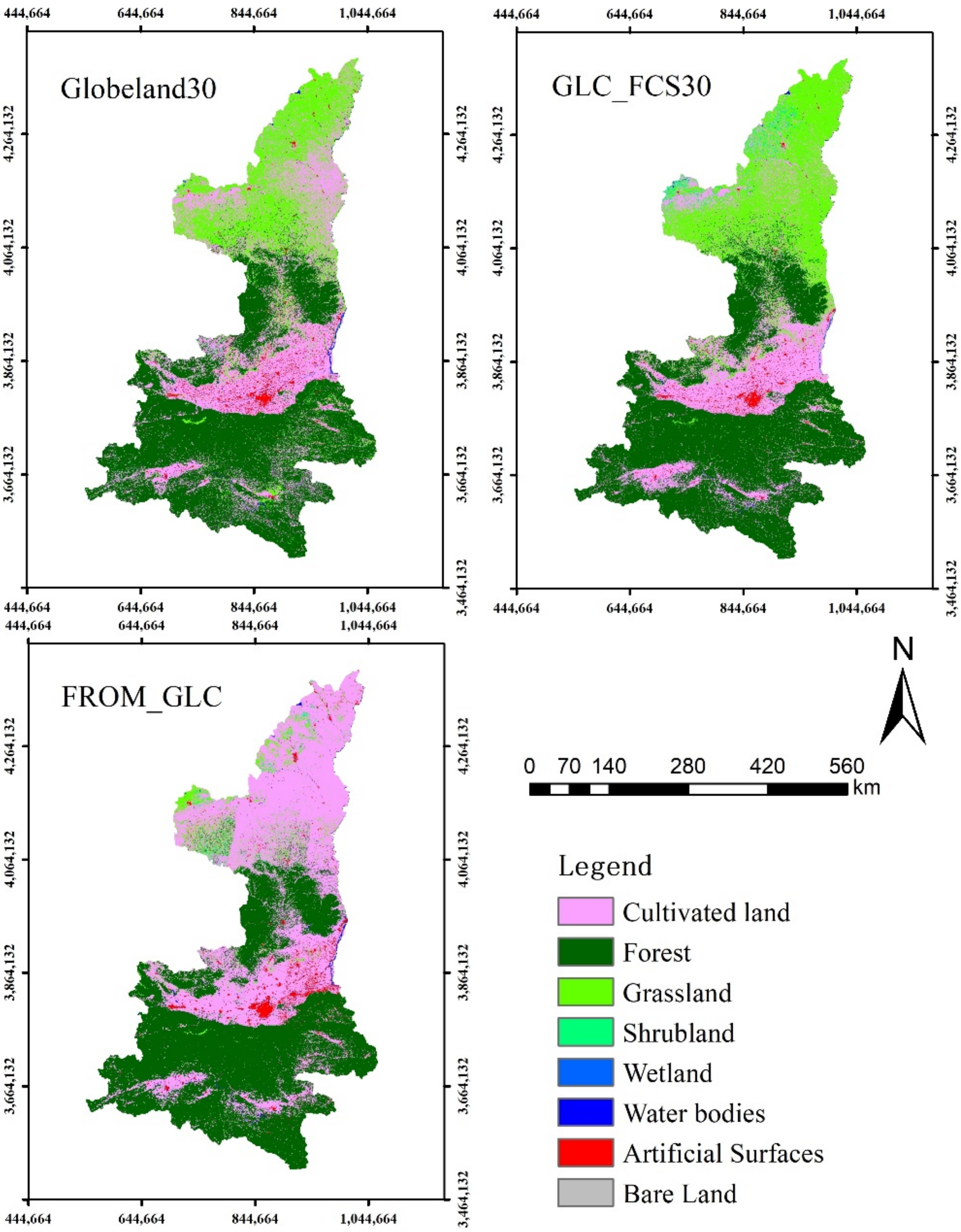

(**a**)

Figure 1. *Cont.*

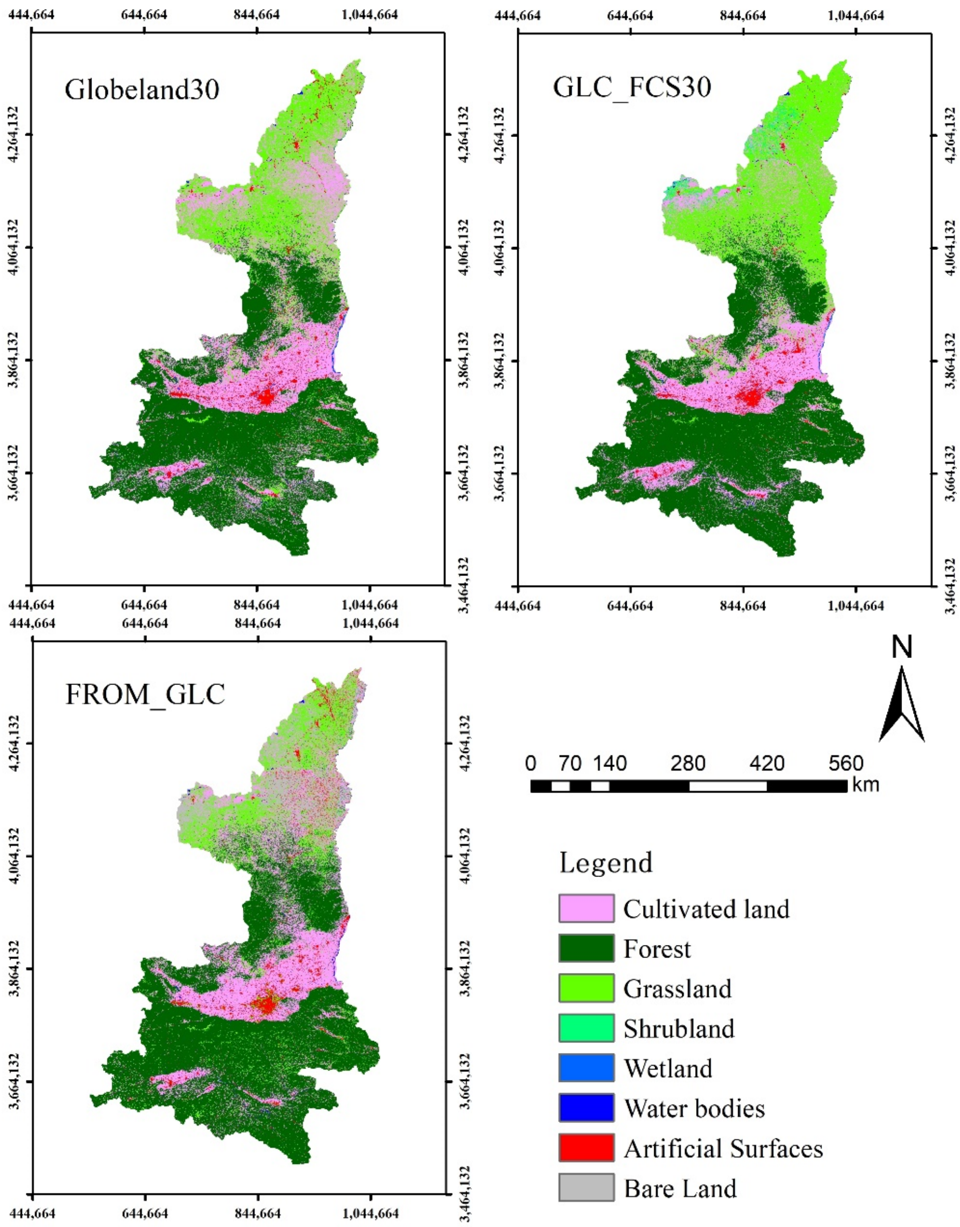

(**b**)

Figure 1. The base land cover maps of Shaanxi province, China, in 2010 (**a**) and 2020 (**b**).

GlobeLand30 (http://www.globallandcover.com/home_en.html (accessed on 10 January 2023)) is a 30 m spatial resolution global land cover product with three versions developed by the National Geomatics Center of China (version 2000 and 2010) and the Ministry of Natural Resources of China (version 2020) [25]. The classification system of GlobeLand30 includes ten level I land cover classes (i.e., cultivated land, forest, grassland, shrubland, wetland, water bodies, tundra, artificial surfaces, bare land, and permanent snow and ice) [25]. There are eight level I land cover classes in the study area (except tundra and permanent snow and ice). In this study, GlobeLand30 was taken as the baseline for quality comparison, and its classification system was used as the classification system of interpretation.

FROM-GLC (Fine Resolution Observation and Monitoring of Global Land Cover) (http://data.ess.tsinghua.edu.cn/ (accessed on 10 January 2023)) is a global land cover product derived from Landsat series sensors. In its early version, the spatial resolution of FROM-GLC was 30 m [26]. However, Sentinel-2 images based FROM-GLC 2017v1 is a 10 m resolution global land cover product [27]. By majority voting, we resampled the FROM-GLC 2017v1 to 30 m in the study area. We used FROM-GLC 2017v1 as a substitute for nominal year 2020.

GLC_FCS30 (https://data.casearth.cn/en/ (accessed on 10 January 2023)) is a global land cover product with a 30 m spatial resolution and a fine classification system that contains 29 land cover classes [5]. Like GlobeLand30 and the early version of FROM-GLC, Landsat TM/ETM+ images were the data source of GLC_FCS30.

Basic information about the three products employed in this research, including classification systems, spatial resolution, data sources, and classification approaches, can be found in [5,25–27]. The number of labels, or the number of classes of the classification systems, was defined by producers. The resolution of the GlobeLand30 and GLC-FCS30 land cover maps is the same as the resolution of Landsat series TM images (i.e., 30 m) used in map production, while the resolution of FROM-GLC 2017v1 is 10 m, the same as its data source, the Sentinel-2 images. The classification approaches of the three base products are rather different. With respect to the classifiers used, the classifier used for GlobaLand30 and FROM_GLC was SVM, and the classifier applied in GLC-FCS30 was RF. More details about the classification processes of base products are given in the references listed above.

Before fusing base products, different classification systems need to be harmonized in the study area for accuracy assessments, although it is not a prerequisite for map fusion by the proposed method, as mentioned in the introduction section. We selected GlobeLand30′s classification system as the default classification system and converted other land cover products to the default classification system in the study area. The mapping of the land cover classes among the different land cover products is shown in Table 1 below.

Table 1. Relating base products' classification systems. Column "Code" in the table is the integer defined to encode class labels in the LC products concerned.

Globeland30 Classes	Code	FROM_GLC Classes	Code	GLC_FCS30 Classes	Code
Cultivated land	10	Cropland	10	Rainfed cropland	10
				Herbaceous cover	11
				Irrigated cropland	20
Forest	20	Forest	20	Open evergreen broadleaved forest	51
				Closed evergreen broadleaved forest	52
				Open deciduous broadleaved forest	61
				Closed deciduous broadleaved forest	62
				Open evergreen needle-leaved forest	71
				Closed evergreen needle-leaved forest	72
				Open deciduous needle-leaved forest	81
				Closed deciduous needle-leaved forest	82
Grassland	30	Grass	30	Grassland	130
Shrubland	40	Shrub	40	Shrubland	120
				Evergreen shrubland	121
				Deciduous shrubland	122
Wetland	50	Wetland	50	Wetlands	180
Water bodies	60	Water	60	Water body	210
Artificial surfaces	80	Impervious	80	Impervious surfaces	190
Bare land	90	Bareland	90	Sparse vegetation	150
				Bare areas	200
				Unconsolidated bare areas	202

2.2. Augmented Sampling and Accuracy Assessment

Samples are collections of individual sample units (i.e., pixels) for modeling and accuracy assessment. As recommended for accuracy assessment [28], we applied stratified random sampling design. Different land cover or land cover change classes are defined as individual strata in conventional stratified random sampling to reduce the estimation variance. Furthermore, setting a minimum stratum sample size guarantees sufficient sample units for rare classes.

To reduce the workload of interpretation, we applied an augmented sampling design, which helped to adjust the sample size of each stratum without violating the principles of the stratified sampling. In augmented sampling design, the final sample set (for a base product) consists of two subsets: the initial baseline sample subset and the augmented sample subset. The initial baseline subset is shared for all base products but augmented subsets are separate for individual base products. The initial baseline sample units were allocated to different cross-strata, defined by both climatic regions and land cover classes. We adjusted the sample size of each cross-strata to keep the inclusion probabilities of sample units from different cross-strata with the same land cover class equal. Some units in the initial baseline sample subset may be randomly removed and some new units need to be randomly added to augmented sample subsets. Therefore, most of sample units in the initial baseline sample subset were shared for different base products in the same year. More details about augmented sampling and sample size adjustment can be found in Appendix A. We list the sample size allocation of the six training samples and six test samples (for three base products in two nominal years) after adjustment in Table 2.

Table 2. Allocation of training sample size to strata of individual base products. Test sample sizes are shown in parentheses.

		Cultivated Land	Forest	Grassland	Shrubland	Wetland	Water Bodies	Artificial Surfaces	Bare Land	Total
Globeland30	2010	143 (143)	202 (201)	115 (115)	51 (50)	50 (50)	51 (50)	52 (52)	51 (51)	715 (712)
	2020	138 (138)	199 (199)	112 (112)	51 (50)	50 (50)	51 (50)	54 (53)	51 (51)	706 (703)
GLC_FCS30	2010	123 (123)	209 (208)	121 (121)	51 (51)	50 (50)	51 (50)	52 (51)	51 (51)	708 (705)
	2020	117 (116)	210 (210)	119 (118)	52 (51)	50 (50)	51 (50)	54 (53)	51 (51)	704 (699)
FROM-GLC	2010	229 (228)	208 (207)	54 (53)	51 (50)	50 (50)	51 (50)	52 (52)	50 (50)	745 (740)
	2020	137 (136)	217 (216)	64 (64)	51 (50)	50 (50)	51 (50)	55 (54)	60 (59)	685 (679)

Accuracy measures, such as OA, UA, and PA, were estimated following the methods detailed in Appendix A. To estimate OA, we defined an indicator $y(u)$ that donates the correctness of the classification at unit (pixel) u. OA, the population mean of y, can be estimated via the indicators of the sample units $y(u)$ and their inclusion probabilities $\pi(u)$. The estimation of UA and PA requires another indicator $x(u)$. By modifying the definitions of $x(u)$, UA and PA can be estimated via the ratio estimator, as described in Appendix A.

2.3. Methods for Multiple Land Cover Product Fusion

2.3.1. Weighting by Localized Map-Reference Cover Type Transition Probabilities (TP)

We propose a method for product fusion using per-pixel map-reference cover type transition probabilities for weighting the source products (thus the method is named TP). By method TP, the probabilities of the land cover class $j = 1, 2, \ldots, I$ at pixel $\mathbf{x}$ are calculated:

$$prob(\mathbf{x})_j = \frac{1}{M} \sum_{m=1}^{M} \sum_{i=1}^{I} a(\mathbf{x})_{mi} p(\mathbf{x})_{mij} \quad (1)$$

where $M = 3$ is the number of the base products, $a(\mathbf{x})_{mi}$ is the areal proportions of map class i (i.e., probability of map class i), and $p(\mathbf{x})_{mij}$ is the transition probability (conditional probability) that the reference class is j given the map class is i, with $\mathbf{x}$ indicating a pixel being analyzed and m indicating a product incorporated for fusion. The areal proportion $a(\mathbf{x})_{mi}$ can be treated as the ith row sum of the base product m from the perspective of a localized error matrix at $\mathbf{x}$. Therefore, the production $a(\mathbf{x})_{mi} p(\mathbf{x})_{mij}$ can be viewed as the ith row and the jth column cell of the aforementioned localized error matrix at pixel $\mathbf{x}$. When $a(\mathbf{x})_{mi}$ and $p(\mathbf{x})_{mij}$ refer to the statistics estimated over map m as a whole, we have the consensus method of Tuanmu and Jetz [23] (named CON).

The per-pixel transition probability that each reference class occurs given a map class is predicted using random forest (RF). For this, there were three types of explanatory variables: map classifications, local landscape indices, and terrain variables. Map classes were the land cover class labels extracted from each base product at the reference sample pixels. Local landscape indices were typical landscape indices, including homogeneity, heterogeneity, entropy, dominance, and contagion, computed in the local moving windows whose sizes were odds varied from 3×3 to 11×11 [29]. Terrain variables derived from digital elevation model (DEM), such as the elevation, aspect, and slope, are also incorporated as explanatory variables for modeling. We used the Shuttle Radar Topography Mission (SRTM) DEMs (30 m resolution) (https://earthexplorer.usgs.gov (accessed on 10 January 2023)) to derive terrain variables. Models were built with explanatory variables mentioned above. Note that elevation, slope, and aspect were shared for all models. The training sample was divided into different subsets (strata) based on the map class.

2.3.2. Random Forest-Based Modeling (RF)

Using this method, reference class occurrences are modeled using reference classifications in reference sample data as response variables and input source map classifications as explanatory variables. Specifically, the explanatory variables include map classifications, local landscape indices computed from map classifications, and terrain variables. We built RF models and fused three land cover products for both 2010 and 2020, using R package: randomForest [30].

2.3.3. Modified Dempster–Shafer (D-S) Method

With this method [20], the frame of discernment $\theta = \{C_1, C_2, \ldots, C_I\}$ corresponded to all candidate land cover classes defined in the classification system. The mass functions (termed basic probability assignment, BPA) were subjected to the flowing conditions:

$$\begin{cases} m_j(\phi; \mathbf{x}) = 0 \\ \sum\limits_{C_i \subseteq \theta} m_j(C_i; \mathbf{x}) = 1 \cdot \end{cases} \tag{2}$$

where $j = 1, 2, 3$ denotes the models corresponding to three different products.

The mass functions in Equation (2) measure the evidence that a pixel belongs to classes C_i's at location $\mathbf{x}$. They were predicted by the RF models built with the reference sample data, as described in Section 2.3.1.

Through the Dempster rule of combination, the sum of all masses was the orthogonal sum of the three mass functions and calculated via:

$$m_1 \bigoplus m_2 \bigoplus m_3(C) = \frac{1}{K} \sum_{C_1 \cap C_2 \cap C_3 = C} m_1(C_1) m_2(C_2) m_3(C_3) \tag{3}$$

and:

$$K = \sum_{C_1 \cap C_2 \cap C_3 \neq \varnothing} m_1(C_1) m_2(C_2) m_3(C_3) \tag{4}$$

is a normalization factor. As $m_j(\phi; \mathbf{x})$, the mass function, is localized, the orthogonal sum was computed locally using R package: EvCombR [31].

Figure 2 shows the flowchart of the general fusion process of the study. The first step is sampling design. We applied an augmented sampling design to select both training samples and test samples. We applied four different methods, including RF, DS, CON, and TP, to fuse multiple land cover products. In the accuracy assessment procedure, accuracy measures were estimated based on test samples for evaluating fusion methods.

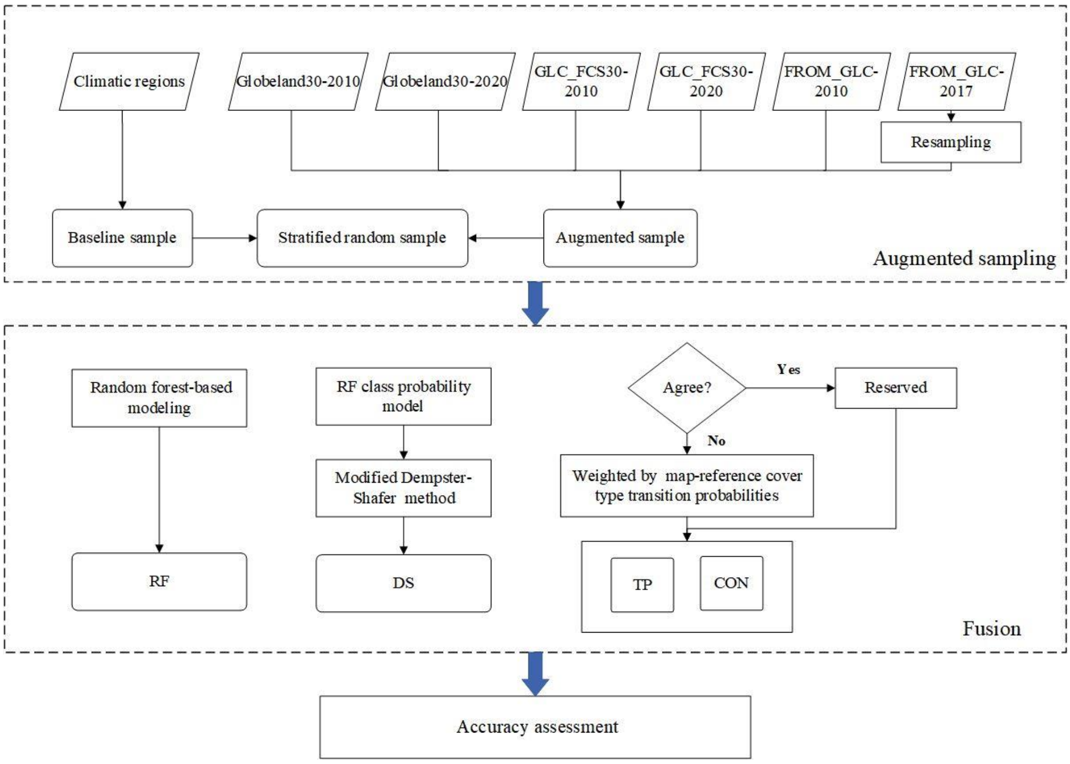

Figure 2. The flowchart of fusion process of the multiple land cover products.

3. Results

3.1. Accuracy Assessment of Base Land Cover Products

Based on the six test samples (shown in Table 2), we assessed the accuracies of all base products used in this research. The error matrices are listed in Tables 3, 5, A2, A4, A6 and A7 in Appendix B. All figures in the error matrices are reported in percentages, i.e., the area proportions of the study area. We summarized UAs and OAs of base products for 2010 and 2020 in Tables 3 and 4, respectively, where SEs are indicated in parentheses.

Table 3. UAs and OAs of base products for 2010.

	UA(SE) (%)								OA(SE) (%)
	Cultivated Land	**Forest**	**Grassland**	**Shrubland**	**Wetland**	**Water Bodies**	**Artificial Surfaces**	**Bare Land**	
GlobeLand30	79.72 (3.37)	92.54 (1.86)	60.00 (4.59)	46.00 (7.12)	44.00 (7.09)	82.00 (5.49)	61.54 (6.81)	62.75 (6.84)	80.80 (1.65)
GLC_FCS30	74.80 (3.93)	91.83 (1.90)	44.63 (4.54)	66.67 (6.67)	44.00 (7.09)	96.00 (2.80)	86.27 (4.87)	43.14 (7.00)	75.33 (1.71)
FROM-GLC	46.05 (3.31)	91.30 (1.96)	50.94 (6.93)	52.00 (7.14)	58.00 (7.05)	82.00 (5.49)	50.00 (7.00)	72.00 (6.41)	68.12 (1.78)

Table 4. UAs and OAs of base products for 2020.

	UA(SE) (%)								OA(SE) (%)
	Cultivated Land	**Forest**	**Grassland**	**Shrubland**	**Wetland**	**Water Bodies**	**Artificial Surfaces**	**Bare Land**	
GlobeLand30	74.64 (3.72)	92.46 (1.88)	55.36 (4.72)	50.00 (7.14)	56.00 (7.09)	78.00 (5.92)	66.04 (6.57)	74.51 (6.16)	78.41 (1.72)
GLC_FCS30	76.72 (3.94)	91.90 (1.89)	59.32 (4.54)	47.06 (7.06)	40.00 (7.00)	98.00 (2.00)	86.79 (4.70)	43.14 (7.00)	79.41 (1.69)
FROM-GLC	59.56 (4.22)	88.43 (2.18)	50.00 (6.30)	30.00 (6.55)	22.00 (5.91)	100.00 (0)	57.41 (6.79)	5.08 (2.88)	67.94 (1.74)

The error matrices indicate that the OAs of GlobeLand30 and GLC_FCS are approximately 0.77~0.81, except for GLC_FCS 2010, whose OA is 0.7533. However, FROM-GLC's OAs are relatively lower (approximately 0.68) compared with other base products in the study area. UAs for the forest are generally approximately 0.90, higher than those of other classes. Grassland, shrubland, wetland, and bare land are classes that are relatively difficult to classify, as their UAs are lower compared with other classes.

3.2. Accuracy Assessment of Fused Land Cover Maps

The accuracy measures were estimated via error matrices, providing the basis to evaluate different fusion methods. The fused maps in the study area were also generated for visualization. Figure 3a shows four fused land cover products for 2010 and 2020, respectively. Figure 4a,b shows two 600 m × 600 m subsets centered at sample units A (2010) and B (2020), respectively.

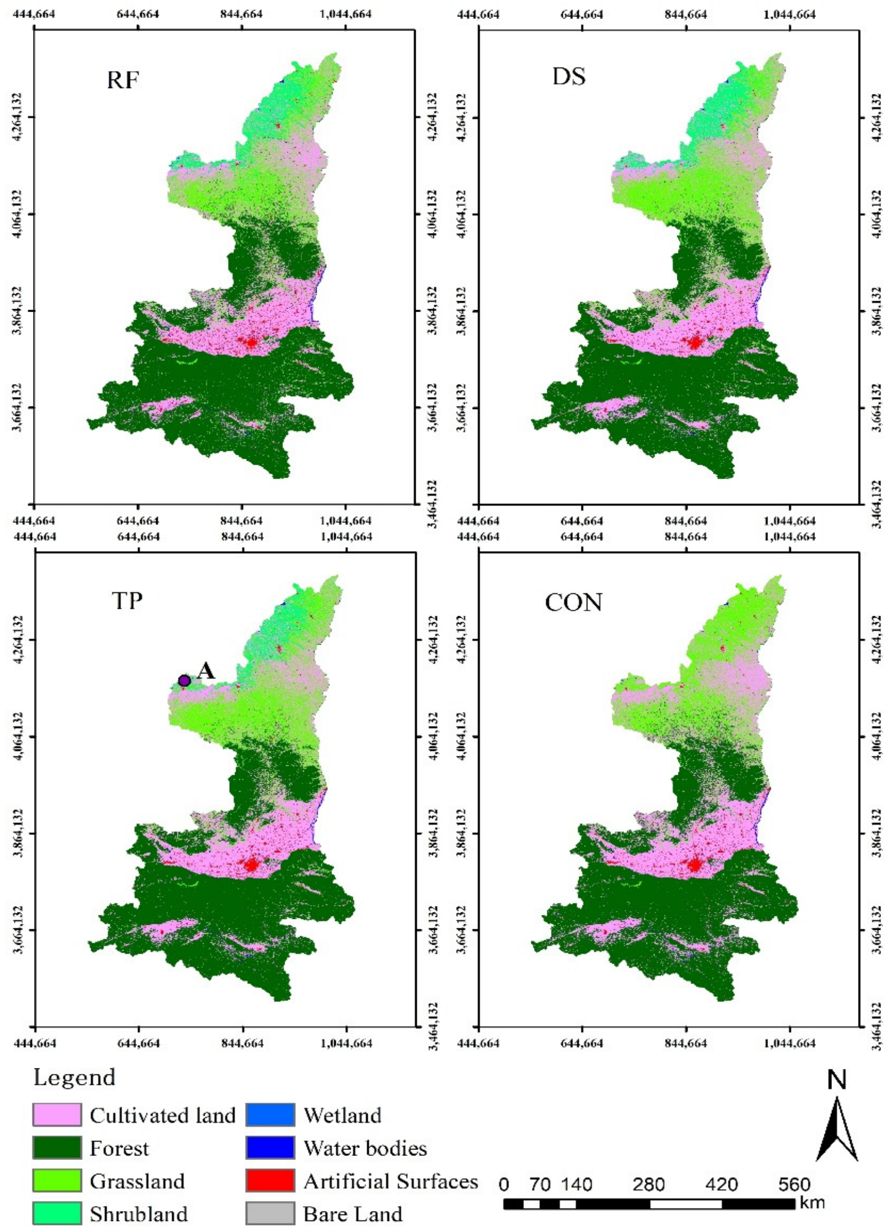

(**a**)

Figure 3. *Cont*.

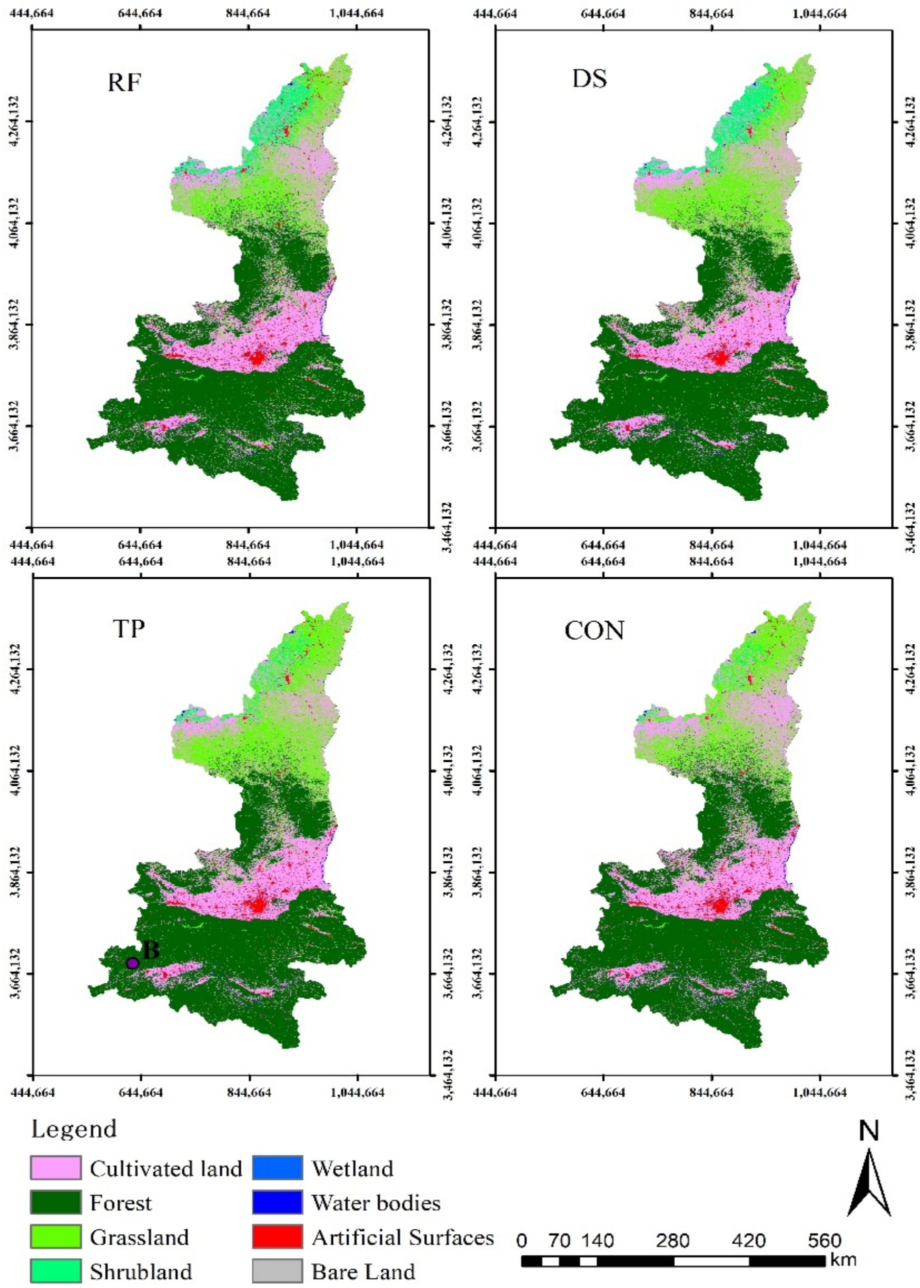

(**b**)

Figure 3. The fused land cover products for 2010 (**a**) and 2020 (**b**).

Methods described in Section 2.3 were applied to fuse multiple land cover products. Accuracy assessment was carried out for the fused products based on the test samples of GlobaLand30 in 2010 and 2020, respectively. Error matrices are shown in Tables A8–A15 in Appendix B. We summarize the gains in UAs and OAs in Tables 5 and 6 below.

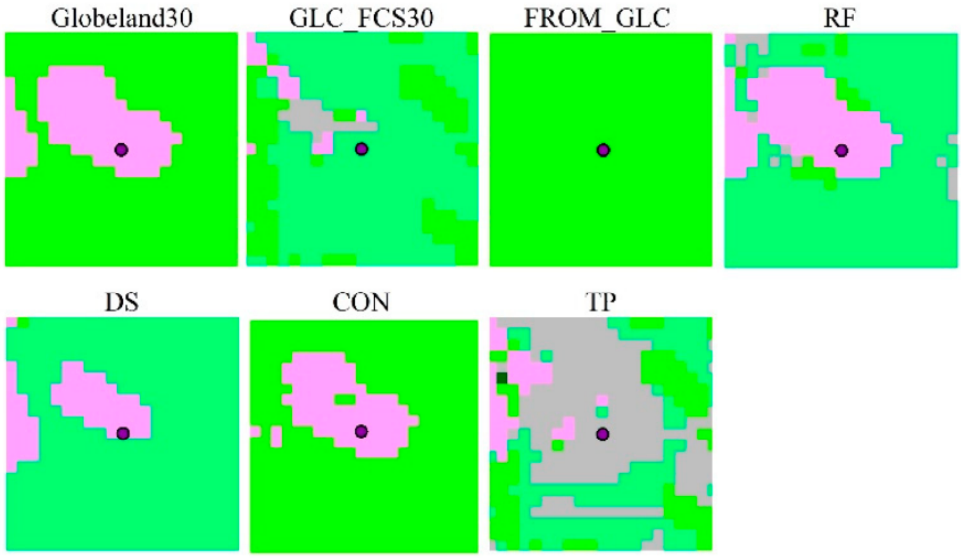

(**a**)

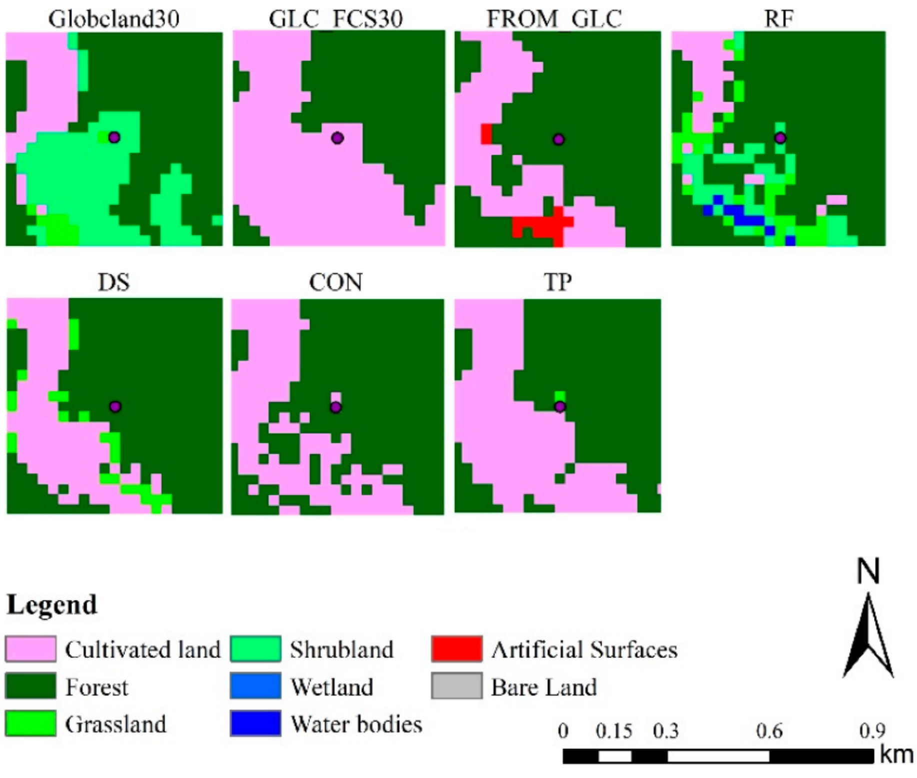

(**b**)

Figure 4. Subsets of base and fused products centered at: (**a**) sample unit A (2010) and (**b**) sample unit B (2020).

Table 5. Accuracy gains in different fusion products, 2010.

	UA (%)								OA (%)
	Cultivated Land	Forest	Grassland	Shrubland	Wetland	Water Bodies	Artificial Surfaces	Bare Land	
RF	2.5	−3.88	17.77	26.33	11.73	−0.4	5.13	−16.13	2.62
D-S	2.49	1.36	17.72	25.37	32.92	8.1	2.86	15.93	4.91
TP	4.75	0.6	16.89	38.3	9.15	7.97	35.02	10.69	6.32
CON	−2.7	−0.82	1.07	−4.2	10.55	−2.37	31.07	2.87	−0.05

Table 6. Accuracy gains in different fusion products, 2020.

	UA (%)								OA (%)
	Cultivated Land	Forest	Grassland	Shrubland	Wetland	Water Bodies	Artificial Surfaces	Bare Land	
RF	4.03	−2.26	15.87	6.28	2.33	−2.62	8.9	5.04	3.57
D-S	6.55	1.68	21.89	17.15	12.42	−1.68	11.99	20.25	7.34
TP	11.61	0.43	25.11	24.71	44	2.07	10.44	24.2	9.29
CON	1.34	−3.54	6.04	−22.28	44	3.5	−1.66	19.24	1.04

As shown in Tables 5 and 6, the OAs of the fused products are higher than any base product in both 2010 and 2020, except for that by CON in 2010. The difference in the OAs between CON and GlobeLand30 in 2010 is negligible because the standard error is 1.64% (Table A12, Appendix B). Among these fusion methods, RF slightly increased the OAs. Moderate improvements in the OAs were achieved using the D-S method enhanced with local mass functions. The largest accuracy gains were achieved using TP, in which local map-reference cover type transition probabilities were used for fusion.

4. Discussion

We discuss the results obtained in this research first, emphasizing the advantages of the proposed method of TP relative to the alternatives. As indicated in the error matrices of base products (Tables A2–A7, Appendix B), more than 85% (even 90%) of the areal proportions in the study area are occupied by cultivated land, forest (approximately 40~50%), and grassland on the land cover maps. Shrubland, wetland, water bodies, artificial surfaces, and bare land are rare classes. Areal proportions are different among three base products, especially for grassland. Approximately 12.76% and 5.75% of the total area was mislabeled as cultivated land by the FROM-GLC in 2010 and 2020, respectively. Confusion between cultivated land and grassland seems to be the major source of commission error of cultivated land. Because of this type of confusion, some pixels whose reference class was grassland were labeled as cultivated land, leading to increased stratum weight but a decreased UA of cultivated land. Equation (A4) in Appendix A implies that the OA estimate is a weighted average of UAs. Thus, those land cover classes with large weight and low UAs would finally reduce OAs. Similarly, forest is the stratum with the largest weight in the study area (0.4467 for 2010 and 0.4455 for 2020), its UA tends to influence OA the most. Although forest UAs are relatively high (approximately 90%), a minor decline in UAs might result in a large reduction of OAs.

Tables 5 and 6 show accuracy gains obtained using different fusion methods. Although gains in OAs were achieved in most cases, this is not the case for UAs, especially those classes whose accuracies were already very high, such as forest and water bodies.

When mass functions were estimated locally, the D-S method appears to be a competitive fusion method, with all UAs increasing except for water bodies in 2020. Since water stratum weight is relatively small in the study area, the impact of the UA decrease is negligible. On the other hand, the considerably increased UAs of shrubland, wetland, and grassland contribute to increased OAs.

Method TP leads to the greatest gains in OAs. Compared with method CON, UAs are all improved, except for forest and water bodies, as their UAs are relatively high in source maps. The difference in accuracy gains between CON and TP demonstrate the advantages of localized transition probabilities for the fusion of land cover information.

In the introductory section, the existing literature on land cover map fusion has already been extensively reviewed with respect to methodological developments. The proposed method TP extends and improves upon the accuracy-based method [23], and the synergistic method involving the use of conditional probabilities [10]. TP was empirically confirmed to outperform the alternative methods. It is applicable for large-area land cover map fusion across the world, although the accuracy gains may be geographically varied.

Further work is needed to refine the proposed method, especially with respect to the way localized transition probabilities are predicted. Comparative performances (in terms of UAs) of the methods compared in this research suggest that complementarity between methods should be explored. Other competing methods for product fusion are also worth exploring (e.g., [32–36]), though a comprehensive comparative study is beyond the scope of this paper. Further work is also needed to overcome larger discrepancy in spatial resolution among base products, though base products in this study are of the same or similar spatial resolutions, given that land cover products are increasingly available with differing spatial resolution, both fine and coarse.

5. Conclusions

This paper presents a novel method for fusing land cover products. It is based on weighting the individual base products by map-reference cover type transition probabilities, which are predicted for individual map pixels using random forest. A study using three kinds of land cover products for Shaanxi Province, China, for 2010 and 2020 was carried out, confirming that the proposed method achieved the greatest gains in OAs (it outperforms other methods by 2~8% in OA gains), while the methods tested all achieved gains in accuracy relative to base products (except for CON in 2010) (the methods lead to gains of 1~9% in OAs). In the proposed method, a localized prediction of the transition probabilities provides fuller information about the weighting of source products for fusion. It is applicable for fusing products with different classification systems (though harmonized classification systems allow for comparative accuracy assessments using error matrices as in this research). In other words, this method is well suited for map fusion even when base products are not produced with the same classification scheme, as transition probabilities are conditional probabilities that candidate reference classes occur given individual map classes, which do not have to refer to the same sets of land cover classes.

Author Contributions: Conceptualization, W.Z. and J.Z.; Funding acquisition, W.Z. and M.C.; Investigation, H.L.; Methodology, W.Z., J.W., Y.W., and J.Z.; Validation, W.Z. and J.W.; Writing—original draft, W.Z.; Writing—review and editing, W.Z. and J.Z. All authors have read and agreed to the published version of the manuscript.

Funding: This research was funded by the Fundamental Research Funds for the Central Universities, CHD, grant number 300102262902, 300102260108. Shaanxi Forestry Science and Technology Innovation Program, grant number SXLK2021-0225.

Conflicts of Interest: The authors declare no conflict of interest.

Appendix A. Accuracy Assessment

Appendix A.1. Sampling Design and Augmented Sampling

Selecting a proper sampling design for multiple land cover products in the study area is challenging because strata defined by any product may not be suitable for other products. Inspired by existing works [37,38], we chose climatic regionalization as the basis of stratification and applied an augmented sampling design because the strata would be independent of any of the land cover products and strata sample sizes can be adjusted flexibly. The Chinese climate map, acquired from the Resource and Environment Science and Data Center (https://www.resdc.cn (accessed on 10 January 2023)), was the climate map we applied. In augmented sampling design, the final sample set for a product (map) consists of two sample subsets: the initial baseline sample subset and the augmented sample subset. The baseline sample subset was a stratified random sample whose strata were climatic regions. By adjusting the sample size of each cross-stratum, the combination of the baseline and the augmented sample subsets led to a stratified random sample whose strata were land cover classes and inclusion probabilities of units in the same stratum are adjusted to be equal.

The first step of the sampling design is sample size estimation. Olofsson et al. [39] recommended stratified random sampling design for area estimation and accuracy assessment and provided the general principles of sample size calculation and allocation for stratified random sampling. Sample size can be estimated via:

$$n = \frac{\left(\sum W_i S_i\right)^2}{\left[S(\hat{O})\right]^2 + 1/N \sum W_i S_i^2} \approx \left(\frac{\sum W_i S_i}{S(\hat{O})}\right)^2 \tag{A1}$$

as suggested [39,40]. In Equation (A1), W_i is the stratum weight of class i (i.e., the areal proportion of class i on the map), $S_i = \sqrt{U_i(1-U_i)}$ is the standard deviation of class i, and U_i is UA of class i. As OA and UA for GlobeLand30 are about 0.7~0.8, we estimated the baseline sample size is approximately 953, assuming the standard deviation of overall accuracy $S(\hat{O})$ is 0.02. In this study, the reference sample data (for a product in one nominal year) consist of two equal-size samples: the training sample and the test sample. Therefore, we doubled the sample size estimated by Equation (A1).

After the estimation of the baseline sample size, the next step is to allocate sample units to each stratum and apply re-stratification. Because the baseline sample is stratified by climatic regions, few baseline sample units may be allocated to the rare classes. We supplied and allocated augmented sample units to all rare classes to ensure that there were at least 100 sample units (50 for training, 50 for test) in each stratum. The inclusion probability of stratum h is calculated by $\pi_h = n_h/N_h$, where n_h is the sample size of land cover class, and N_h is the total number of pixels belong to class h on the map. The sample size of every cross-strata was adjusted according to π_h. Table A1 shows the sample adjustments of GlobeLand30 2010, for example.

Table A1. Sample size adjustments for GlobeLand30 2010.

InitialStratum (*h*)	Land Cover Class (*j*)								TOTAL
	Cultivated Land	Forest	Grassland	Shrubland	Wetland	Water Bodies	Artificial Surfaces	Bare Land	
IIIC1	61 (−4)	41 (+7)	84 (+2)	0 (+5)	0 (+23)	0 (+13)	0 (+5)	0 (+2)	186 (−4) (+57)
IIIB3	143 (−12)	206 (+1)	27 (−6)	0 (+53)	1 (+44)	2 (+35)	15 (+74)	0 (+1)	394 (−18) (+208)
IVA2	41 (+1)	155 (−8)	12 (−3)	1 (+20)	0 (+8)	0 (+32)	0 (+5)	0 (0)	209 (−11) (+66)
IIC1	20 (+15)	0 (+1)	70 (−3)	1 (+12)	0 (+8)	1 (+9)	2 (+1)	3 (+30)	97 (−3) (+76)
IIC2	21 (0)	1 (−1)	37 (+10)	0 (+9)	0 (+16)	2 (+7)	1 (+1)	5 (+61)	67 (−1) (+104)
TOTAL	286 (−16) (+16)	403 (−9) (+9)	230 (−12) (+12)	2 (+99)	1 (+99)	5 (+96)	18 (+86)	8 (+94)	953 (−37) (+511)

Appendix A.2. Response Design and Analysis

The response design aims to establish protocols to determine the agreement between map classifications and reference classifications. We used pixels as the basic interpret units, and a 30 m buffer was generated for each sample pixel. Based on Google Earth high-resolution images, the interpreter labeled reference classes without consulting the map classifications of land cover products. The dominate class in the buffer was defined as the reference class of the sample unit. When multiple classes were present in the buffer and no dominated class was found, the reference condition at the center pixel was assigned as the reference class.

In the analysis process, we applied different estimators to estimate accuracies. When we estimated OA, an indicator $y(u)$ was defined as:

$$y(u) = \begin{cases} 1, \; map\ class\ matches\ reference\ class \\ 0, otherwise \end{cases} \tag{A2}$$

where u donates a sample unit. OA is estimated via:

$$\hat{\hat{Y}} = \frac{1}{N} \sum_{u \in s} \frac{y(u)}{\pi_u} \tag{A3}$$

where π_u is the inclusion probability of sample unit u, N is the population size, and s represents the sample set. For stratified random sampling, Equation (A3) can be rewritten as:

$$\hat{\hat{Y}} = \frac{1}{N} \sum_{h=1}^{H} \sum_{u=1}^{n_h} \frac{y(u)}{\pi_h} = \sum_{h=1}^{H} W_h \overline{y}_h \tag{A4}$$

where H is the number of strata, n_h is the sample size of stratum h, $W_h = n_h/N_h$ is the stratum weight and $\overline{y}_h$ is the stratum mean, which is also the estimator of UA of class h marked as $\hat{U}_h$. The variance estimator of OA is:

$$\hat{V} = \sum_{h=1}^{H} W_h^2 \hat{U}_h (1 - \hat{U}_h)/(n_h - 1). \tag{A5}$$

Variance and its square root, i.e., standard error, should also be reported in the accuracy assessment for estimating 95% CI ($\hat{\hat{Y}} \pm 1.96\sqrt{\hat{V}}$). If the cell in the ith row and jth column of an error matrix is the survey parameter to be estimated, Equation (A2) can be redefined as:

$$y(u) = \begin{cases} 1, map\ class\ label\ is\ i\ and\ reference\ class\ label\ is\ j \\ 0, otherwise \end{cases}. \tag{A6}$$

By modifying the definitions of the indicators $x(u)$ and $y(u)$, we can estimate the UA and producer's accuracy (PA) via the ratio estimator. In this study, we focus on OA and its variance. More details about applying the ratio estimator to estimate the UA and PA (and their variance) can be found in other research [28,41].

Appendix B. Error Matrices of Base and Fused Land Cover Products

In Appendix B, we list the error matrices of three base products (Tables A2–A7) and fused land cover products (Tables A8–A15) in 2010 and 2020. All figures in the error matrices are reported in percentages, i.e., the area proportions of the study area and SEs of UAs, PAs, and OAs are indicated in parentheses, respectively.

Table A2. Error matrix of GlobeLand30 2010.

Map	Reference								TOTAL	UA (SE)
	Cultivated Land	Forest	Grassland	Shrubland	Wetland	Water Bodies	Artificial Surfaces	Bare Land		
Cultivated land	24.91	1.53	3.06	0.44	0.00	0.44	0.66	0.22	31.25	79.72 (3.37)
Forest	1.11	41.34	2.22	0.00	0.00	0.00	0.00	0.00	44.67	92.54 (1.86)
Grassland	2.51	0.36	12.36	4.84	0.00	0.00	0.18	0.36	20.60	60.00 (4.59)
Shrubland	0.03	0.02	0.03	0.07	0.00	0.00	0.01	0.00	0.16	46.00 (7.12)
Wetland	0.02	0.00	0.00	0.01	0.05	0.03	0.00	0.00	0.11	44.00 (7.09)
Water bodies	0.00	0.02	0.02	0.00	0.04	0.33	0.00	0.00	0.41	82.00 (5.49)
Artificial surfaces	0.54	0.00	0.12	0.17	0.00	0.00	1.33	0.00	2.16	61.54 (6.81)
Bare land	0.00	0.00	0.00	0.24	0.00	0.00	0.00	0.40	0.64	62.75 (6.84)
TOTAL	29.12	43.26	17.82	5.76	0.09	0.81	2.17	0.98		
PA(SE)	85.57 (2.44)	95.55 (1.37)	69.36 (4.37)	1.27 (0.27)	54.86 (11.34)	41.26 (15.84)	61.22 (12.04)	41.16 (14.26)		80.80 (1.65)

Table A3. Error matrix of GLC_FCS30 2010.

Map	Reference								TOTAL	UA (SE)
	Cultivated Land	Forest	Grassland	Shrubland	Wetland	Water Bodies	Artificial Surfaces	Bare Land		
Cultivated land	18.42	1.40	3.00	0.00	0.20	0.20	1.20	0.20	24.62	74.80 (3.93)
Forest	1.58	43.24	2.26	0.00	0.00	0.00	0.00	0.00	47.09	91.83 (1.90)
Grassland	5.34	1.38	10.68	5.73	0.00	0.00	0.59	0.20	23.93	44.63 (4.54)
Shrubland	0.24	0.00	0.05	0.82	0.00	0.00	0.00	0.12	1.24	66.67 (6.67)
Wetland	0.01	0.00	0.00	0.00	0.04	0.05	0.00	0.00	0.10	44.00 (7.09)
Water bodies	0.00	0.00	0.00	0.00	0.00	0.21	0.00	0.00	0.22	96.00 (2.80)
Artificial surfaces	0.13	0.03	0.00	0.00	0.03	0.00	1.42	0.03	1.65	86.27 (4.87)
Bare land	0.20	0.00	0.00	0.45	0.00	0.00	0.00	0.50	1.16	43.14 (7.00)
TOTAL	25.92	46.06	16.00	7.01	0.28	0.46	3.21	1.05		
PA(SE)	71.05 (3.18)	93.87 (1.49)	66.76 (4.79)	11.76 (1.88)	15.91 (11.66)	45.89 (20.15)	44.18 (8.20)	47.45 (13.59)		75.33 (1.71)

Table A4. Error matrix of FROM_GLC 2010.

Map	Reference								TOTAL	UA(SE)
	Cultivated Land	Forest	Grassland	Shrubland	Wetland	Water Bodies	Artificial Surfaces	Bare Land		
Cultivated land	20.62	2.95	12.76	5.50	0.00	0.00	1.77	1.18	44.77	46.05 (3.31)
Forest	2.76	43.51	1.38	0.00	0.00	0.00	0.00	0.00	47.65	91.30 (1.96)
Grassland	0.43	0.22	1.95	0.72	0.00	0.22	0.00	0.29	3.82	50.94 (6.93)
Shrubland	0.08	0.05	0.24	0.41	0.00	0.00	0.00	0.02	0.80	52.00 (7.14)
Wetland	0.00	0.01	0.00	0.00	0.03	0.01	0.00	0.00	0.05	58.00 (7.05)
Water bodies	0.01	0.02	0.01	0.00	0.03	0.38	0.01	0.01	0.46	82.00 (5.49)
Artificial surfaces	0.65	0.14	0.33	0.00	0.05	0.00	1.22	0.05	2.43	50.00 (7.00)
Bare land	0.00	0.00	0.00	0.00	0.00	0.00	0.00	0.01	0.01	72.00 (6.41)
TOTAL	24.56	46.88	16.67	6.63	0.11	0.61	2.99	1.55		
PA(SE)	83.95 (2.93)	92.80 (1.49)	11.69 (1.74)	6.23 (1.23)	28.87 (13.42)	62.64 (12.76)	40.61 (8.55)	0.67 (0.22)		68.12 (1.78)

Table A5. Error matrix of GloabLand30 2020.

Map	Reference								TOTAL	UA (SE)
	Cultivated Land	Forest	Grassland	Shrubland	Wetland	Water Bodies	Artificial Surfaces	Bare Land		
Cultivated land	23.12	3.14	3.37	0.22	0.22	0.22	0.45	0.22	30.97	74.64 (3.72)
Forest	0.90	41.20	2.46	0.00	0.00	0.00	0.00	0.00	44.55	92.46 (1.88)
Grassland	1.96	1.78	11.06	3.75	0.00	0.00	0.18	1.25	19.98	55.36 (4.72)
Shrubland	0.02	0.02	0.03	0.08	0.00	0.00	0.01	0.00	0.15	50.00 (7.14)
Wetland	0.02	0.00	0.00	0.00	0.07	0.03	0.00	0.00	0.12	56.00 (7.09)
Water bodies	0.02	0.02	0.01	0.00	0.04	0.33	0.01	0.00	0.42	78.00 (5.92)
Artificial surfaces	0.66	0.00	0.24	0.12	0.00	0.00	2.11	0.06	3.19	66.04 (6.57)
Bare land	0.00	0.00	0.00	0.13	0.00	0.01	0.01	0.45	0.60	74.51 (6.16)
TOTAL	26.69	46.16	17.17	4.30	0.34	0.60	2.76	1.98		
PA(SE)	86.62 (2.47)	89.24 (1.88)	64.42 (4.58)	1.77 (0.41)	20.49 (13.90)	55.45 (20.95)	76.23 (10.19)	22.54 (6.03)		78.41 (1.72)

Table A6. Error matrix of GLC_FCS 2020.

Map	Reference								TOTAL	UA (SE)
	Cultivated Land	Forest	Grassland	Shrubland	Wetland	Water Bodies	Artificial Surfaces	Bare Land		
Cultivated land	18.34	2.47	1.44	0.21	0.00	0.41	1.03	0.00	23.90	76.72 (3.94)
Forest	0.90	43.40	2.92	0.00	0.00	0.00	0.00	0.00	47.22	91.90 (1.89)
Grassland	3.98	1.39	13.91	3.58	0.00	0.00	0.40	0.20	23.45	59.32 (4.54)
Shrubland	0.42	0.00	0.05	0.63	0.00	0.00	0.03	0.21	1.34	47.06 (7.06)
Wetland	0.00	0.00	0.00	0.00	0.06	0.07	0.00	0.00	0.14	40.00 (7.00)
Water bodies	0.00	0.00	0.00	0.00	0.01	0.25	0.00	0.00	0.26	98.00 (2.00)
Artificial surfaces	0.27	0.05	0.00	0.00	0.00	0.00	2.45	0.05	2.83	86.79 (4.70)
Bare land	0.37	0.00	0.03	0.07	0.02	0.00	0.00	0.37	0.86	43.14 (7.00)
TOTAL	24.27	47.32	18.36	4.49	0.08	0.74	3.91	0.83		
PA(SE)	75.55 (3.08)	91.72 (1.66)	75.76 (4.16)	14.09 (3.12)	71.59 (16.64)	34.31 (13.45)	62.76 (8.64)	44.39 (12.25)		79.41 (1.69)

Table A7. Error matrix of GLC_FROM 2020.

Map	Reference								TOTAL	UA (SE)
	Cultivated Land	**Forest**	**Grassland**	**Shrubland**	**Wetland**	**Water Bodies**	**Artificial Surfaces**	**Bare Land**		
Cultivated land	15.03	2.23	5.75	0.93	0.00	0.37	0.56	0.37	25.23	59.56 (4.22)
Forest	2.28	43.60	3.42	0.00	0.00	0.00	0.00	0.00	49.31	88.43 (2.18)
Grassland	1.56	1.56	6.23	2.72	0.00	0.00	0.19	0.19	12.46	50.00 (6.30)
Shrubland	0.01	0.05	0.12	0.08	0.00	0.00	0.00	0.00	0.25	30.00 (6.55)
Wetland	0.00	0.00	0.00	0.00	0.00	0.01	0.00	0.00	0.01	22.00 (5.91)
Water bodies	0.00	0.00	0.00	0.00	0.00	0.41	0.00	0.00	0.41	100.00 (0)
Artificial surfaces	0.49	0.14	0.77	0.07	0.14	0.00	2.17	0.00	3.77	57.41 (6.79)
Bare land	2.90	0.29	2.76	1.89	0.00	0.00	0.29	0.44	8.56	5.08 (2.88)
TOTAL	22.27	47.87	19.05	5.68	0.14	0.78	3.21	1.00		
PA(SE)	67.48 (3.52)	91.09 (1.60)	32.70 (3.64)	1.33 (0.35)	1.44 (17.33)	51.91 (17.33)	67.53 (9.33)	43.49 (19.87)		67.94 (1.74)

Table A8. Error matrix of fused product 2010 using random forest.

Map	Reference								TOTAL	UA (SE)
	Cultivated Land	**Forest**	**Grassland**	**Shrubland**	**Wetland**	**Water Bodies**	**Artificial Surfaces**	**Bare Land**		
Cultivated land	23.49	0.66	2.59	0.48	0.00	0.22	0.91	0.22	28.57	82.22 (3.25)
Forest	2.86	41.55	2.18	0.05	0.00	0.23	0.00	0.00	46.87	88.66 (2.11)
Grassland	1.65	1.03	12.58	0.91	0.00	0.01	0.00	0.00	16.17	77.77 (4.48)
Shrubland	0.55	0.01	0.38	3.99	0.00	0.00	0.18	0.40	5.51	72.33 (7.92)
Wetland	0.00	0.00	0.00	0.01	0.04	0.02	0.00	0.00	0.07	55.73 (9.88)
Water bodies	0.00	0.01	0.02	0.00	0.05	0.33	0.00	0.00	0.41	81.60 (5.08)
Artificial surfaces	0.37	0.00	0.08	0.08	0.00	0.00	1.08	0.00	1.62	66.67 (7.62)
Bare land	0.18	0.00	0.00	0.24	0.00	0.00	0.00	0.37	0.78	46.62 (11.99)
TOTAL	29.12	43.26	17.82	5.76	0.09	0.81	2.17	0.98		
PA(SE)	80.67 (3.09)	96.05 (1.34)	70.60 (4.54)	69.20 (7.60)	43.94 (11.10)	41.09 (15.80)	49.74 (10.67)	37.30 (13.10)		83.42 (1.61)

Table A9. Error matrix of fused product 2020 using random forest.

Map	Reference								TOTAL	UA(SE)
	Cultivated Land	**Forest**	**Grassland**	**Shrubland**	**Wetland**	**Water Bodies**	**Artificial Surfaces**	**Bare Land**		
Cultivated land	23.00	0.67	3.85	0.29	0.22	0.22	0.75	0.22	29.24	78.67 (3.51)
Forest	1.75	43.99	3.00	0.02	0.00	0.00	0.00	0.00	48.77	90.20 (1.98)
Grassland	1.12	1.47	9.11	0.73	0.00	0.00	0.00	0.36	12.79	71.23 (5.41)
Shrubland	0.37	0.01	1.08	3.09	0.00	0.00	0.01	0.93	5.49	56.28 (8.87)
Wetland	0.01	0.00	0.00	0.00	0.05	0.02	0.00	0.00	0.09	58.33 (8.30)
Water bodies	0.02	0.02	0.01	0.00	0.06	0.34	0.01	0.00	0.45	75.38 (5.70)
Artificial surfaces	0.42	0.00	0.12	0.06	0.00	0.00	1.99	0.06	2.65	74.94 (6.58)
Bare land	0.00	0.00	0.00	0.09	0.00	0.01	0.00	0.41	0.52	79.55 (6.14)
TOTAL	26.69	46.16	17.17	4.30	0.34	0.60	2.76	1.98		
PA(SE)	86.19 (2.79)	95.29 (1.33)	53.05 (4.90)	71.90 (8.67)	15.37 (10.56)	56.68 (21.41)	71.99 (10.08)	20.76 (5.64)		81.98 (1.65)

Table A10. Error matrix of fused product 2010 using modified Dempster–Shafer.

Map	Reference								TOTAL	UA (SE)
	Cultivated Land	**Forest**	**Grassland**	**Shrubland**	**Wetland**	**Water Bodies**	**Artificial Surfaces**	**Bare Land**		
Cultivated land	24.04	0.84	2.33	0.55	0.02	0.24	0.99	0.23	29.24	82.21 (3.11)
Forest	1.33	41.78	1.33	0.01	0.00	0.04	0.00	0.00	44.50	93.90 (1.67)
Grassland	2.57	0.64	13.57	0.65	0.00	0.02	0.00	0.01	17.45	77.72 (4.31)
Shrubland	0.72	0.00	0.54	4.39	0.00	0.01	0.18	0.32	6.16	71.37 (7.50)
Wetland	0.00	0.00	0.00	0.00	0.02	0.01	0.00	0.00	0.03	76.92 (11.80)
Water bodies	0.00	0.00	0.01	0.00	0.04	0.49	0.00	0.00	0.55	90.10 (5.13)
Artificial surfaces	0.47	0.00	0.04	0.04	0.00	0.00	1.00	0.00	1.55	64.40 (11.31)
Bare land	0.00	0.00	0.00	0.11	0.00	0.00	0.00	0.42	0.53	78.68 (9.35)
TOTAL	29.12	43.26	17.82	5.76	0.09	0.81	2.17	0.98		
PA(SE)	82.56 (3.04)	96.58 (1.26)	76.14 (4.40)	76.29 (6.88)	24.94 (7.82)	60.96 (19.87)	45.91 (10.2)	42.71 (16.62)		85.71 (1.50)

Table A11. Error matrix of fused product 2020 using modified Dempster–Shafer.

Map	Reference								TOTAL	UA(SE)
	Cultivated Land	Forest	Grassland	Shrubland	Wetland	Water Bodies	Artificial Surfaces	Bare Land		
Cultivated land	23.95	1.84	1.95	0.30	0.24	0.24	0.75	0.23	29.49	81.19 (3.22)
Forest	0.68	43.19	1.98	0.02	0.00	0.00	0.00	0.00	45.87	94.14 (1.62)
Grassland	1.39	1.12	12.58	0.57	0.01	0.02	0.06	0.54	16.28	77.25 (4.49)
Shrubland	0.36	0.00	0.54	3.34	0.00	0.00	0.00	0.74	4.97	67.15 (8.52)
Wetland	0.00	0.00	0.00	0.00	0.03	0.01	0.00	0.00	0.05	68.42 (10.77)
Water bodies	0.02	0.02	0.01	0.00	0.05	0.32	0.01	0.00	0.42	76.32 (5.83)
Artificial surfaces	0.30	0.00	0.12	0.06	0.00	0.00	1.92	0.06	2.47	78.03 (6.65)
Bare land	0.00	0.00	0.00	0.01	0.00	0.00	0.01	0.43	0.45	94.76 (4.15)
TOTAL	26.69	46.16	17.17	4.30	0.34	0.60	2.76	1.98		
PA(SE)	89.72 (2.52)	93.55 (1.55)	73.25 (4.67)	77.69 (8.10)	9.51 (6.74)	53.79 (20.47)	69.62 (9.62)	21.46 (9.10)		85.75 (1.48)

Table A12. Error matrix of fused product 2010 using consensus-based method.

Map	Reference								TOTAL	UA(SE)
	Cultivated Land	Forest	Grassland	Shrubland	Wetland	Water Bodies	Artificial Surfaces	Bare Land		
Cultivated land	26.01	1.73	3.43	0.76	0.01	0.44	0.95	0.45	33.78	77.02 (3.22)
Forest	0.89	41.52	2.77	0.02	0.01	0.05	0.00	0.00	45.27	91.72 (1.88)
Grassland	2.20	0.01	11.58	4.76	0.00	0.02	0.18	0.22	18.96	61.07 (4.74)
Shrubland	0.00	0.00	0.00	0.04	0.00	0.00	0.00	0.05	0.09	41.80 (18.45)
Wetland	0.00	0.00	0.00	0.00	0.01	0.01	0.00	0.00	0.02	54.55 (15.16)
Water bodies	0.01	0.01	0.00	0.00	0.05	0.28	0.00	0.00	0.35	79.63 (5.16)
Artificial surfaces	0.00	0.00	0.04	0.04	0.00	0.00	1.04	0.00	1.12	92.61 (5.07)
Bare land	0.00	0.00	0.00	0.14	0.00	0.00	0.00	0.26	0.40	65.62 (8.48)
TOTAL	29.12	43.26	17.82	5.76	0.09	0.81	2.17	0.98		
PA(SE)	89.35 (2.38)	95.98 (1.37)	64.98 (4.69)	0.66 (0.38)	14.96 (6.10)	34.88 (13.63)	47.97 (10.46)	27.01 (9.98)		80.75 (1.64)

Table A13. Error matrix of fused product 2010 using localized transition probabilities.

Map	Reference								TOTAL	UA(SE)
	Cultivated Land	Forest	Grassland	Shrubland	Wetland	Water Bodies	Artificial Surfaces	Bare Land		
Cultivated land	24.23	0.22	2.20	0.97	0.02	0.23	0.78	0.04	28.69	84.47 (2.99)
Forest	1.77	42.62	1.29	0.05	0.00	0.02	0.00	0.00	45.76	93.14 (1.71)
Grassland	2.93	0.42	14.10	0.79	0.00	0.02	0.04	0.04	18.34	76.89 (4.23)
Shrubland	0.18	0.00	0.00	3.93	0.00	0.00	0.18	0.37	4.66	84.30 (6.33)
Wetland	0.00	0.00	0.00	0.00	0.03	0.02	0.00	0.00	0.05	53.15 (16.47)
Water bodies	0.00	0.01	0.00	0.00	0.04	0.51	0.00	0.00	0.57	89.97 (4.83)
Artificial surfaces	0.00	0.00	0.04	0.00	0.00	0.00	1.16	0.00	1.21	96.56 (3.41)
Bare land	0.00	0.00	0.18	0.01	0.00	0.00	0.00	0.54	0.73	73.44 (20.88)
TOTAL	29.12	43.26	17.82	5.76	0.09	0.81	2.17	0.98		
PA(SE)	83.23 (3.07)	98.51 (0.82)	79.14 (4.19)	68.22 (7.86)	28.98 (10.11)	63.53 (20.07)	53.71 (11.16)	54.72 (16.87)		87.12 (1.44)

Table A14. Error matrix of fused product 2020 using consensus-based method.

Map	Reference								TOTAL	UA(SE)
	Cultivated Land	Forest	Grassland	Shrubland	Wetland	Water Bodies	Artificial Surfaces	Bare Land		
Cultivated land	23.30	1.90	3.54	0.38	0.02	0.23	0.83	0.46	30.67	75.98 (3.41)
Forest	1.80	43.91	3.64	0.02	0.00	0.01	0.00	0.00	49.37	88.92 (2.06)
Grassland	1.12	0.36	9.65	3.69	0.00	0.02	0.06	0.82	15.72	61.40 (5.14)
Shrubland	0.00	0.00	0.00	0.20	0.00	0.00	0.00	0.52	0.73	27.72 (20.36)
Wetland	0.00	0.00	0.00	0.00	0.02	0.00	0.00	0.00	0.02	100.00 (0)
Water bodies	0.01	0.00	0.00	0.00	0.06	0.32	0.00	0.00	0.40	81.50 (5.14)
Artificial surfaces	0.47	0.00	0.34	0.00	0.22	0.00	1.87	0.00	2.90	64.38 (10.23)
Bare land	0.00	0.00	0.00	0.00	0.00	0.01	0.00	0.18	0.19	93.75 (6.11)
TOTAL	26.69	46.16	17.17	4.30	0.34	0.60	2.76	1.98		
PA(SE)	87.31 (2.84)	95.11 (1.41)	56.21 (4.85)	4.70 (4.09)	5.85 (4.35)	53.87 (20.51)	67.66 (9.32)	8.90 (2.98)		79.45 (1.70)

Table A15. Error matrix of fused product 2020 using localized transition probabilities.

Map	Reference								TOTAL	UA(SE)
	Cultivated Land	Forest	Grassland	Shrubland	Wetland	Water Bodies	Artificial Surfaces	Bare Land		
Cultivated land	23.30	1.68	1.09	0.09	0.02	0.24	0.59	0.00	27.02	86.25 (2.85)
Forest	1.13	44.08	2.16	0.02	0.00	0.00	0.06	0.00	47.46	92.89 (1.72)
Grassland	2.01	0.40	13.25	0.41	0.00	0.00	0.00	0.38	16.47	80.47 (4.28)
Shrubland	0.00	0.00	0.54	3.70	0.00	0.01	0.00	0.70	4.95	74.71 (7.84)
Wetland	0.00	0.00	0.00	0.00	0.02	0.00	0.00	0.00	0.02	100.00 (0)
Water bodies	0.01	0.00	0.01	0.00	0.06	0.34	0.01	0.00	0.43	80.07 (5.32)
Artificial surfaces	0.24	0.00	0.12	0.06	0.22	0.00	2.10	0.00	2.75	76.48 (8.53)
Bare land	0.00	0.00	0.00	0.01	0.00	0.00	0.00	0.90	0.91	98.71 (1.37)
TOTAL	26.69	46.16	17.17	4.30	0.34	0.60	2.76	1.98		
PA(SE)	87.30 (2.84)	95.49 (1.37)	77.18 (4.45)	86.10 (5.97)	6.59 (4.82)	57.26 (21.71)	75.99 (8.47)	45.40 (13.27)		87.70 (1.42)

References

1. Loveland, T.; Belward, A. The IGBP-DIS Global 1-Km Land Cover Data Set, DIScover: First Results. *Int. J. Remote Sens.* **1997**, *18*, 3289–3295. [CrossRef]
2. Bartholomé, E.; Belward, A. GLC2000: A New Approach to Global Land Cover Mapping from Earth Observation Data. *Int. J. Remote Sens.* **2005**, *26*, 1959–1977. [CrossRef]
3. Friedl, M.; Sulla-Menashe, D.; Tan, B.; Schneider, A.; Ramankutty, N.; Sibley, A.; Huang, X. MODIS Collection 5 Global Land Cover: Algorithm Refinements and Characterization of New Datasets. *Remote Sens. Environ.* **2010**, *114*, 168–182. [CrossRef]
4. Yang, J.; Huang, X. The 30 m Annual Land Cover Dataset and Its Dynamics in China from 1990 to 2019. *Earth Syst. Sci. Data* **2021**, *13*, 3907–3925. [CrossRef]
5. Zhang, X.; Liu, L.; Chen, X.; Gao, Y.; Xie, S.; Mi, J. GLC_FCS30: Global Land-Cover Product with Fine Classification System at 30 m Using Time-Series Landsat Imagery. *Earth Syst. Sci. Data* **2021**, *13*, 2753–2776. [CrossRef]
6. Liu, H.; Gong, P.; Wang, J.; Wang, X.; Ning, G.; Xu, B. Production of Global Daily Seamless Data Cubes and Quantification of Global Land Cover Change from 1985 to 2020—IMap World 1.0. *Remote Sens. Environ.* **2021**, *258*, 112364. [CrossRef]
7. Fritz, S.; See, L. Identifying and Quantifying Uncertainty and Spatial Disagreement in the Comparison of Global Land Cover for Different Applications. *Glob. Chang. Biol.* **2008**, *14*, 1057–1075. [CrossRef]
8. Nelson, M.D.; Garner, J.D.; Tavernia, B.G.; Stehman, S.V.; Riemann, R.I.; Lister, A.J.; Perry, C.H. Assessing Map Accuracy from a Suite of Site-Specific, Non-Site Specific, and Spatial Distribution Approaches. *Remote Sens. Environ.* **2021**, *260*, 112442. [CrossRef]
9. Jung, M.; Henkel, K.; Herold, M.; Churkina, G. Exploiting Synergies of Global Land Cover Products for Carbon Cycle Modeling. *Remote Sens. Environ.* **2006**, *101*, 534–553. [CrossRef]
10. Pérez-Hoyos, A.; García-Haro, F.J.; San-Miguel-Ayanz, J. A Methodology to Generate a Synergetic Land-Cover Map by Fusion of Different Land-Cover Products. *Int. J. Appl. Earth Obs. Geoinf.* **2012**, *19*, 72–87. [CrossRef]
11. Herold, M.; Mayaux, P.; Woodcock, C.E.; Baccini, A.; Schmullius, C. Some Challenges in Global Land Cover Mapping: An Assessment of Agreement and Accuracy in Existing 1 Km Datasets. *Remote Sens. Environ.* **2008**, *112*, 2538–2556. [CrossRef]
12. McCallum, I.; Obersteiner, M.; Nilsson, S.; Shvidenko, A. A Spatial Comparison of Four Satellite Derived 1 km Global Land Cover Datasets. *Int. J. Appl. Earth Obs. Geoinf.* **2006**, *8*, 246–255. [CrossRef]
13. Li, Z.; White, J.C.; Wulder, M.A.; Hermosilla, T.; Davidson, A.M.; Comber, A.J. Land Cover Harmonization Using Latent Dirichlet Allocation. *Int. J. Geogr. Inf. Sci.* **2021**, *35*, 348–374. [CrossRef]
14. Pérez-Hoyos, A.; Udías, A.; Rembold, F. Integrating Multiple Land Cover Maps through a Multi-Criteria Analysis to Improve Agricultural Monitoring in Africa. *Int. J. Appl. Earth Obs. Geoinf.* **2020**, *88*, 102064. [CrossRef] [PubMed]

15. Kinoshita, T.; Iwao, K.; Yamagata, Y. Creation of a Global Land Cover and a Probability Map through a New Map Integration Method. *Int. J. Appl. Earth Obs. Geoinf.* **2014**, *28*, 70–77. [CrossRef]
16. See, L.; Schepaschenko, D.; Lesiv, M.; McCallum, I.; Fritz, S.; Comber, A.; Perger, C.; Schill, C.; Zhao, Y.; Maus, V.; et al. Building a Hybrid Land Cover Map with Crowdsourcing and Geographically Weighted Regression. *Int. Soc. Photogramm. Remote Sens. J. Photogramm. Remote Sens.* **2015**, *103*, 48–56. [CrossRef]
17. Tsendbazar, N.-E.; de Bruin, S.; Fritz, S.; Herold, M. Spatial Accuracy Assessment and Integration of Global Land Cover Datasets. *Remote Sens.* **2015**, *7*, 15804–15821. [CrossRef]
18. Tsendbazar, N.-E.; de Bruin, S.; Herold, M. Integrating Global Land Cover Datasets for Deriving User-Specific Maps. *Int. J. Digit. Earth* **2017**, *10*, 219–237. [CrossRef]
19. Lesiv, M.; Moltchanova, E.; Schepaschenko, D.; See, L.; Shvidenko, A.; Comber, A.; Fritz, S. Comparison of Data Fusion Methods Using Crowdsourced Data in Creating a Hybrid Forest Cover Map. *Remote Sens.* **2016**, *8*, 261. [CrossRef]
20. Ran, Y.H.; Li, X.; Lu, L.; Li, Z.Y. Large-Scale Land Cover Mapping with the Integration of Multi-Source Information Based on the Dempster–Shafer Theory. *Int. J. Geogr. Inf. Sci.* **2012**, *26*, 169–191. [CrossRef]
21. Li, B.; Xu, X.; Liu, X.; Shi, Q.; Zhuang, H.; Cai, Y.; He, D. An Improved Global Land Cover Mapping in 2015 with 30 m Resolution (GLC-2015) Based on a Multi-Source Product Fusion Approach. *Earth Syst. Sci. Data Discuss.* **2022**, *2022*, 1–35. [CrossRef]
22. Huang, A.; Shen, R.; Li, Y.; Han, H.; Di, W.; Hagan, D.F. A Methodology to Generate Integrated Land Cover Data for Land Surface Model by Improving Dempster-Shafer Theory. *Remote Sens.* **2022**, *14*, 972. [CrossRef]
23. Tuanmu, M.-N.; Jetz, W. A Global 1-Km Consensus Land-Cover Product for Biodiversity and Ecosystem Modelling. *Glob. Ecol. Biogeogr.* **2014**, *23*, 1031–1045. [CrossRef]
24. Nabil, M.; Zhang, M.; Wu, B.; Bofana, J.; Elnashar, A. Constructing a 30m African Cropland Layer for 2016 by Integrating Multiple Remote Sensing, Crowdsourced, and Auxiliary Datasets. *Big Earth Data* **2022**, *6*, 54–76. [CrossRef]
25. Chen, J.; Chen, J.; Liao, A.; Cao, X.; Chen, L.; Chen, X.; He, C.; Han, G.; Peng, S.; Lu, M.; et al. Global Land Cover Mapping at 30 m Resolution: A POK-Based Operational Approach. *Int. Soc. Photogramm. Remote Sens. J. Photogramm. Remote Sens.* **2015**, *103*, 7–27. [CrossRef]
26. Gong, P.; Wang, J.; Yu, L.; Zhao, Y.; Zhao, Y.; Liang, L.; Niu, Z.; Huang, X.; Fu, H.; Liu, S. Finer Resolution Observation and Monitoring of Global Land Cover: First Mapping Results with Landsat TM and ETM+ Data. *Int. J. Remote Sens.* **2013**, *34*, 2607–2654. [CrossRef]
27. Gong, P.; Liu, H.; Zhang, M.; Li, C.; Wang, J.; Huang, H.; Clinton, N.; Ji, L.; Li, W.; Bai, Y.; et al. Stable Classification with Limited Sample: Transferring a 30-m Resolution Sample Set Collected in 2015 to Mapping 10-m Resolution Global Land Cover in 2017. *Sci. Bull.* **2019**, *64*, 370–373. [CrossRef]
28. Stehman, S.V.; Foody, G.M. Key Issues in Rigorous Accuracy Assessment of Land Cover Products. *Remote Sens. Environ.* **2019**, *231*, 111199. [CrossRef]
29. Zhang, J.; Yang, W.; Zhang, W.; Wang, Y.; Liu, D.; Xiu, Y. An Explorative Study on Estimating Local Accuracies in Land-Cover Information Using Logistic Regression and Class-Heterogeneity-Stratified Data. *Remote Sens.* **2018**, *10*, 1581. [CrossRef]
30. Liaw, A.; Wiener, M. Classification and Regression by RandomForest. *R News* **2002**, *2*, 18–22.
31. Karlsson, A. *EvCombR—Evidence Combination in R*; CRAN: Vienna, Austria, 2022.
32. Gengler, S.; Bogaert, P. Combining Land Cover Products Using a Minimum Divergence and a Bayesian Data Fusion Approach. *Int. J. Geogr. Inf. Sci.* **2018**, *32*, 806–826. [CrossRef]
33. Xu, G.; Chen, B. Generating a Series of Land Covers by Assimilating the Existing Land Cover Maps. *Int. Soc. Photogramm. Remote Sens.J. Photogramm. Remote Sens.* **2019**, *147*, 206–214. [CrossRef]
34. Di Curzio, D.; Castrignanò, A.; Fountas, S.; Romić, M.; Viscarra Rossel, R.A. Multi-Source Data Fusion of Big Spatial-Temporal Data in Soil, Geo-Engineering and Environmental Studies. *Sci. Total Environ.* **2021**, *788*, 147842. [CrossRef]
35. Zhu, X.; Cai, F.; Tian, J.; Williams, T.K. Spatiotemporal Fusion of Multisource Remote Sensing Data: Literature Survey, Taxonomy, Principles, Applications, and Future Directions. *Remote Sens.* **2018**, *10*, 527. [CrossRef]
36. Zhu, L.; Jin, G.; Gao, D. Integrating Land-Cover Products Based on Ontologies and Local Accuracy. *Information* **2021**, *12*, 236. [CrossRef]
37. Olofsson, P.; Stehman, S.V.; Woodcock, C.E.; Sulla-Menashe, D.; Sibley, A.M.; Newell, J.D.; Friedl, M.A.; Herold, M. A Global Land-Cover Validation Data Set, Part I: Fundamental Design Principles. *Int. J. Remote Sens.* **2012**, *33*, 5768–5788. [CrossRef]
38. Stehman, S.V.; Olofsson, P.; Woodcock, C.E.; Herold, M.; Friedl, M.A. A Global Land-Cover Validation Data Set, II: Augmenting a Stratified Sampling Design to Estimate Accuracy by Region and Land-Cover Class. *Int. J. Remote Sens.* **2012**, *33*, 6975–6993. [CrossRef]
39. Olofsson, P.; Foody, G.M.; Herold, M.; Stehman, S.V.; Woodcock, C.E.; Wulder, M.A. Good Practices for Estimating Area and Assessing Accuracy of Land Change. *Remote Sens. Environ.* **2014**, *148*, 42–57. [CrossRef]

40. Cochran, W.G. *Sampling Techniques*, 3rd ed.; John Wiley & Sons: New York, NY, USA, 1977; ISBN 047116240X.
41. Stehman, S.V.; Czaplewski, R.L. Design and Analysis for Thematic Map Accuracy Assessment: Fundamental Principles. *Remote Sens. Environ.* **1998**, *64*, 331–344. [CrossRef]